

Research Project 1-085851

Parametric investigation of a hybrid motor with a helical port

Sagi Dinisman

Advisors:

Prof. Alon Gany

Nachum E. Eisen

Faculty of Aerospace Engineering, Technion – Israel Institute of
Technology

August 2022

Contents

List of Figures.....	3
Abstract.....	4
1. Introduction	5
1.1 Regression rate of hybrid rocket	6
1.1.1 Multiple Fuel Port Geometry	8
1.1.2 Fuel Additives-Aluminum	9
1.1.3 Liquefying Fuels	10
1.1.4 Expandable Graphite	11
1.1.5 Helical Fuel Port.....	13
2. Experimental set-up and test procedure	15
2.1 Casting Helical Fuel Port.....	15
2.2 Experiment Set-Up.....	16
3. Experimental Results	18
3.1 Method 1- Helix Plane.....	19
3.2 Method 2- Straight Port Analogy	21
3.3 Method 3- Grain Parameters	22
4. Conclusions.....	25
References	26

List of Figures

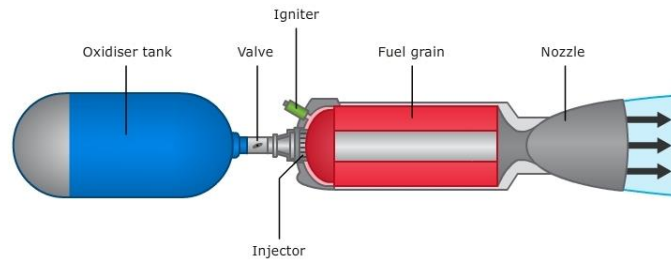
Fig. 1 Schematic of a hybrid rocket system. [1].....	5
Fig. 2 Illustration of hybrid combustion within a boundary layer. [2].....	8
Fig. 3 Multiple port and single port design [6].....	8
Fig. 4 Vacuum Isp and O/F ratio for various concentrations of aluminum mixed with paraffin burning with N_2O_4 . [6].....	9
Fig. 5 schematic of the entrainment mechanism [10].....	10
Fig. 6 Schematic of polymeric fuel matrix with EG heat transfer mechanism during hybrid combustion. [17].....	12
Fig. 7 Process occurring on the surface of polyester fuel containing 3% EG, during flame. [19].....	12
Fig. 8 Regression rate comparison for straight-bore and different helical structures. [21].....	14
Fig. 9 (left) Helical fuel port casting mold; (right) Casted fuel mix, upper row plain polyester, bottom row polyester with 5% EG.	15
Fig. 10 Dissolving the casting mold.....	16
Fig. 11 Schematic description of the helix shape parameters. [26].....	17
Fig. 12 Photograph of the test set up used for static firing experiments.	17
Fig. 13 Post burn photo of Plain polyester (left) and polyester and 5% EG (right) with helical port.	18
Fig. 14 Schematic drawing of the volumetric calculation	19
Fig. 15 Schematic description of lead angle.....	20
Fig. 16 regression rate r vs oxidizer (oxygen) mass flux G_{ox} for polyester with a helical port, polyester and 5% EG with a helical port, and polyester with a straight cylindrical port. Using helix plane method.	23
Fig. 17 regression rate r vs oxidizer (oxygen) mass flux G_{ox} for polyester with a helical port, polyester and 5% EG with a helical port, and polyester with a straight cylindrical port. Using straight port analogy method.....	23
Fig. 18 regression rate r vs oxidizer (oxygen) mass flux G_{ox} for polyester with a helical port, polyester and 5% EG with a helical port, and polyester with a straight cylindrical port. Using grain parameters method.	24

Abstract

Hybrid rockets can be a good propulsion alternative to solid and liquid rockets, due to the combination of safety, low cost, “green”, and high energetic performance. However, the characteristic low regression rate, implying low thrust, is a main drawback in the development of hybrid rocket systems. The improvement of the regression rate with multiple fuel port geometry, fuel additives such as aluminum, and liquefying fuels shows promising results, but these techniques have their disadvantages. A fairly new approach of changing the fuel port to a helical shape is presented in this paper. A series of firing tests with the use of gaseous oxygen as the oxidizer and plain polyester fuel grain with a helical port, showed an increase of up to 2.5 fold in the regression rate compared to a regular straight cylindrical port. Moreover, the addition of 5% expandable graphite to the polyester fuel grain was studied, and showed an increase of 3-fold in the regression rate. By taking into account only the overall fuel grain size, even larger increase in the effective regression rate was noticed, up to 4-folds for plain polyester and 6-fold for 5% EG additive. The enhancement in the regression rate along with the longer internal flow path implies substantially higher fuel mass flow rate from a given fuel grain enabling remarkable increase in the motor thrust or noticeable shortening of the fuel grain and motor. It results with a lighter and smaller rocket motor with improved performance.

1. Introduction

Hybrid motor configuration seeks to combine the advantages of both solid and liquid rockets, by having a combination of solid fuel and liquid or gaseous oxidizer, Fig. 1.



© Copyright. 2011. University of Waikato. All Rights Reserved.

Fig. 1 Schematic of a hybrid rocket system. [1]

The history of hybrid rocket development began in the early 1930s. Even though it was at about the same time of the initial development of both solid and liquid rockets, the level of application and use of hybrid rockets remained significantly smaller. An overview and history of hybrid propulsion is presented in detail by Altman and Holzman (2007) [2].

For liquid bipropellant rocket, leakage and failure in the pump and tank structure can lead to unwanted explosion. In solid rocket, the oxidizer and the fuel are mixed together within a polymer binder. Defects in the propellant can cause uncontrolled combustion.

Storing the oxidizer as a liquid or gas and the fuel as a solid, produces a design in which there is no chance for mixing between the fuel and the oxidizer due to accidental spillage, meaning that hybrid motors are less prone to uncontrolled combustion and explosion.

The safety feature of the hybrid rockets, due to their nonexplosive nature, and separate inert propellant ingredients, leads to safe manufacturing, transportation and handling, which reduces the total operation costs.

Another important attribute for hybrid propulsion is the option of environmentally friendly propellant. In addition, hybrid rocket has the ability to simply control the thrust and apply shutdown and restart, due to the need of controlling only the oxidizer flow rate.

The use of liquid oxidizers, which possess high energetic characteristics

compared to solid oxidizers, yields energetic performance superior to solid rockets and comparable to liquid rockets.

The combination of safety, low cost, “green”, and high energetic performance, makes the hybrid propulsion a good alternative for large launch boosters, especially in the emerging field of space tourism. For instance, the launching of SpaceShipOne in 2004 as the first manned private space flight, Sharp (2019) [3] and SpaceShipTwo, Howell (2019) [4].

Nevertheless, hybrid rockets are more complex than classic solid rockets, and typically have lower performance compared to liquid bipropellant rockets. The biggest drawback in hybrid rockets with polymeric fuels, is the fact that they have low characteristic regression rate, usually an order of magnitude lower than common solid rockets. Low regression rate leads to low thrust levels, which is a significant disadvantage for the use of hybrid rockets as space launch boosters.

More detailed overview on hybrid rocket advantages, disadvantages and characteristics are displayed in [2],[5],[6].

1.1 Regression rate of hybrid rocket

Unlike solid rockets, in which regression rate is strongly coupled to the chamber pressure, hybrid rockets have little to no dependence on chamber pressure, and are correlated to the oxidizer mass flux (G_{ox}).

An analytical regression rate expression was first delivered by Marxman and Gilbert (1963) [7]. The expression assumes analogy between the enthalpy and momentum boundary layers (so-called Reynolds Analogy), the impact of blowing on reducing the heat flux, the use of a total effective heat of vaporization, and the contribution of radiation coupled with convection. Schematic of the hybrid combustion within the boundary layer is shown in Fig. 2.

The fundamental analysis of fuel regression rate as derived from Reynolds Analogy assumes forced convection heat transfer through the boundary layer, between the flame and the gasifying fuel surface as follows:

Heat transfer to the wall is expressed by,

$$q = h(T_f - T_w) \quad (1)$$

where T_f is the flame temperature, and T_w is the wall temperature.

The heat transfer coefficient, h , can be related to Nusselt number Nu ,

$$Nu = \frac{hd}{k} \quad (2)$$

For turbulent flow the Nusselt number can be expressed in term of Reynolds Re and Prandtl Pr numbers,

$$Nu = 0.037Re^{0.8}Pr^{\frac{1}{3}} \quad (3)$$

$$Re = \frac{\rho ud}{\mu} \quad (4)$$

$$Pr = \frac{C_p \mu}{k} \quad (5)$$

where d is the average port diameter, k is the thermal conductivity, ρ is the density, u is the gas velocity, μ is the viscosity, and C_p is the specific heat capacity. All these properties are related to the flowing gases.

Reynold number can be calculated from the overall gas mass flux G ,

$$Re = \frac{Gd}{\mu} \quad (6)$$

The total heat transferred to the surface causes gasification of the fuel,

$$q = \dot{r} \rho_f H_{v,eff} \quad (7)$$

$$\dot{r} = \frac{q}{\rho_f H_{v,eff}} \quad (8)$$

Where $H_{v,eff}$ is the effective heat of vaporization or gasification of the solid fuel, and ρ_f is the density of the fuel.

Combining the equations above, resulting in the fuel regression rate,

$$\begin{aligned} \dot{r} &= \frac{h(T_f - T_w)}{\rho_f H_{v,eff}} = 0.037 \cdot \frac{G^{0.8} \cdot k^{\frac{2}{3}} \cdot C_p^{\frac{1}{3}}}{\rho_f \cdot H_{v,eff} \cdot d^{0.2} \cdot \mu^{0.8 - \frac{1}{3}}} (T_f - T_w) = \\ &= C \cdot \frac{G^{0.8}}{d^{0.2} \cdot H_{v,eff}} (T_f - T_w) \end{aligned} \quad (9)$$

Where C is a constant depending on k , ρ , μ and C_p .

Since the oxidizer mass flux is known (in contrast to the overall mass flux), in practice, a commonly used empirical formula for the fuel regression rate, based on the oxidizer mass flux (G_{ox}), is applied,

$$\dot{r} = a \cdot (G_{ox})^n \quad (10)$$

Where a and n are empirically fitted constants. In general, some dependence on the port size d may be noticed (Eq. (9)). However, when dealing with a specific system, this parameter is not apparent. It indicates however lower regression rate for larger systems.

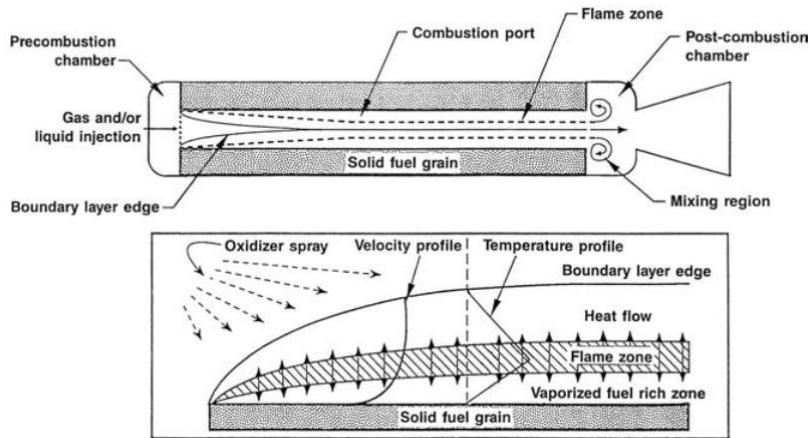


Fig. 2 Illustration of hybrid combustion within a boundary layer. [2]

1.1.1 Multiple Fuel Port Geometry

Most common way used today in the design of space-launch hybrid boosters for enhancement of the overall fuel flow rate, is multiple fuel port or “wagon wheel” geometry, as shown in Fig. 3.

By using multiport or “wagon wheel” geometry, the burning area of the fuel increases significantly, leading to an increase in the thrust level.

However, multiport geometry leads to reduced volumetric loading, due to the larger voids. In addition, there is a significant potential for uneven port burning which compromises fuel grain integrity, especially toward the end of the burn. In contrast to solid propellant, hybrid propellant with wagon wheel geometry possesses greater amount of residuals. The mass of residual has to be considered as “dead mass” that affects the performance of the hybrid motor. If hybrid propellants with a high regression rate exist, then with a single port geometry, the amount of residuals may be very low, Calabro (2011) [5]



Fig. 3 Multiple port and single port designs [6]

1.1.2 Fuel Additives-Aluminum

By using solid fuel, the addition of fuel additives is simple compared to liquid fuel. Performance enhancement materials such as aluminum powder, have high heat of reaction which can slightly increase the specific impulse (I_{sp}) of the rocket. More importantly, fuel additives increase the fuel density.

Evans et al. (2003 [8], 2005 [9]), measured the increase of regression rate due to the addition of aluminum, and showed up to 60% increase in the regression rate for paraffin fuel. Furthermore, Fig. 4 shows the effect of aluminum on the shift of the peak in I_{sp} to lower oxygen to fuel (O/F) ratio. This effect allows the designer to reduce the mass fraction of the oxidizer. Smaller fraction of oxidizer mass can lead to reduction in the size of the oxidizer tank, and simplifying the design of the rocket, Cantwell et al. (2010) [6]

On the other hand, with addition of aluminum, fuel grain strength may be reduced, and there can be losses associated with incomplete combustion of the aluminum. Moreover, by introducing nanosized metal particles motor production costs is higher, and it is more difficult to achieve uniform fuel grain material properties.

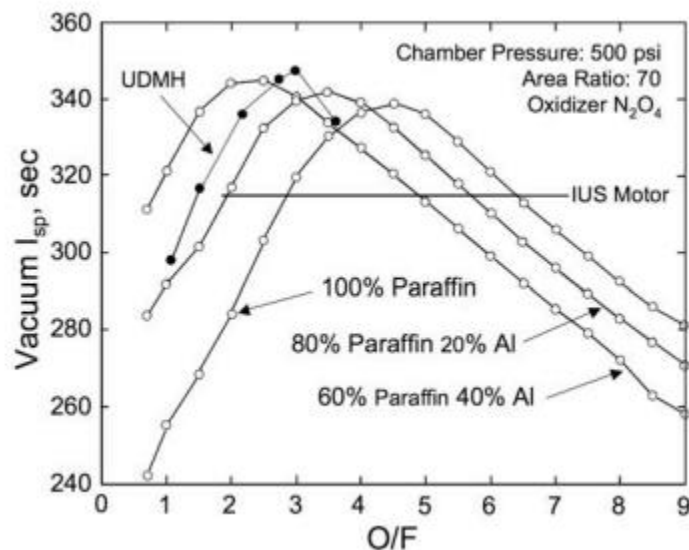


Fig. 4 Vacuum I_{sp} and O/F ratio for various concentrations of aluminum mixed with paraffin burning with N_2O_4 . [6]

1.1.3 Liquefying Fuels

Liquefying fuels, especially paraffin wax, are characterized by substantially higher regression rates than polymeric fuels, hence they can be a good direction for avoiding the use of complex multiport grain configuration.

The most extensive experimental and theoretical work on paraffin fuels has been conducted at Stanford University by Karabeyoglu et al. (2001 [10], 2002 [11], 2004 [12]) and Karabeyoglu and Cantwell (2002) [13]. They investigated an additional mechanism contributing to the overall regression rate. They found that in addition to the mass transfer by gasification of the fuel, liquid fuel droplets are torn from the melt layer forming on the surface due to the shear stress caused by the gas flow over it, resulting in mass transfer entrained into the gas free stream. A schematic of the suggested model is shown in Fig. 5. Work in this subject also carried out at the Technion-Israel Institute of Technology. Weinstein and Gany (2011) [14] proposed an additional mechanism, the mass loss due to liquid melt flowing along the grain. This mechanism accounts for significant mass loss, as well as reduction in motor efficiency in paraffin fuels. Ben-Basat (Sisi) and Gany (2015 [15], 2016 [16]) conducted theoretical and experimental investigation accounting for the existence of liquid melt layer as well as the blowing effect on the heat transfer to the surface, for paraffin fuel and nitrous oxide oxidizer.

Even though paraffin shows large increase in the regression rate, because of the fuel drop entrainment, unburned materials are ejected from the nozzle, and combustion efficiencies for paraffin-based fuels are typically lower. More significantly, it has poor mechanical properties. This means it is unlikely that plain paraffin is applicable in large scale motors. Paraffin-polymer mixed fuel has been studied [[14]-[15]] and, while not achieving the same increase in regression rate as plain paraffin, it can obtain much better mechanical properties.

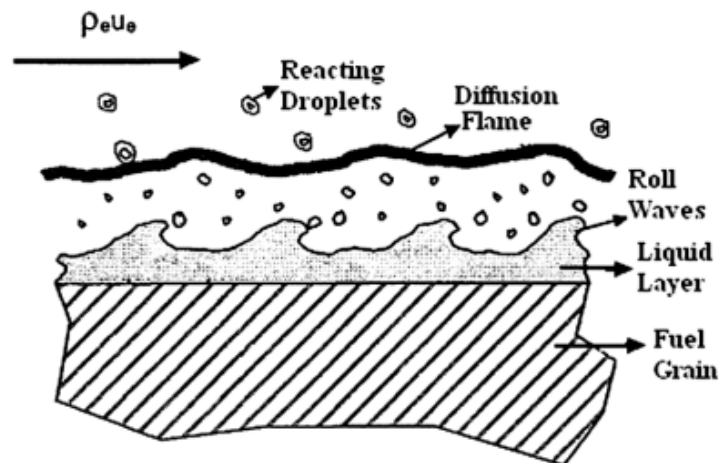


Fig. 5 schematic of the entrainment mechanism [10]

1.1.4 Expandable Graphite

Expandable graphite (EG) is an intercalated form of graphite. It is usually provided as particles / flakes of a typical size of 100-500 micrometer. At elevated temperature (typically above 180°C), it starts to swell, forming wormlike strings several folds longer than the original particles size. EG properties include high thermal conductivity, corrosion resistance, softness, and compression resilience.

Elanjickal and Gany (2020) [17] hypothesized that at the specific conditions of hybrid combustion, EG can be used to enhance the regression rate. When approaching the high temperature zone near the burning surface, the EG particles elongate forming strings whose tips may protrude above the surface, increasing the heat transfer from the hot gases near the surface into the bulk via conduction. The thermal conductivity of EG is several orders of magnitude higher than that of typical solid fuels (paraffin, polyester), meaning that even a small fraction of EG can have a noticeable impact on the regression rate. Schematic illustration of a polymeric fuel matrix with EG additive and the heat transfer mechanisms during hybrid combustion is presented in Fig. 6.

Elanjickal and Gany (2020) [17] derived theoretical model and conducted experiments revealing that in the case of polyester, the addition of 5% EG caused an increase of 100-200% in regression rate and up to 50% increase for paraffin. To show better the penetration and growth of expandable graphite fibers during combustion, Muller and Gany (2020) [18] conducted high-speed photography of a polymeric fuel subjected to flame at atmospheric conditions. Their results support the hypothesis of increase in heat transfer to the fuel via conduction. A series of snapshots taken from a high-speed video movie of a fuel containing 3% EG is presented in Fig. 7 by Muller and Gany (2022) [19]. The figure demonstrates the dynamics of processes occurring on the burning surface, implied by the variation of the EG strings position, shape, and glowing.

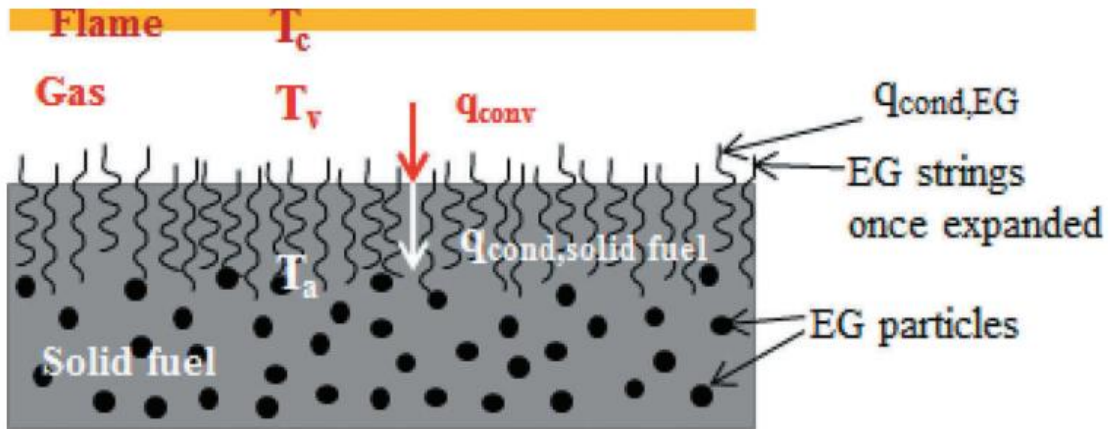


Fig. 6 Schematic of polymeric fuel matrix containing EG particles and the heat transfer mechanisms during hybrid combustion. [17]

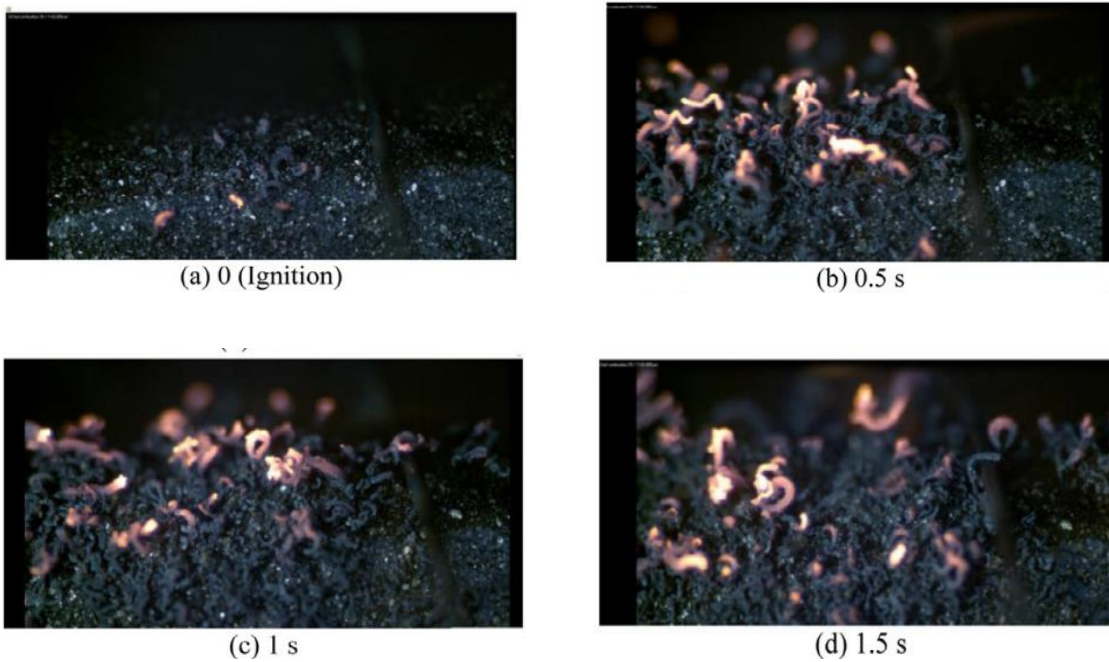


Fig. 7 Process occurring on the surface of polyester fuel containing 3% EG, during flame. [19]

1.1.5 Helical Fuel Port

The rise in the quality level and the price reduction for three dimensional (3-D) printing in recent years, allowed the fabrication of complex port geometries for rocket engines. With the aim to increase the fuel regression rate, new port design features need to increase the surface skin friction and minimize the blowing effect. Blowing effect occurs due to surface ablation which pushing the flame zone away from the fuel surface, resulting in reduction of the convective heat transfer.

Helical fuel port can fit well for hybrid rockets, because helical flows contribute centrifugal component into the flow field. Centrifugal component has the effect of thinning the surface boundary layer, bringing the flame zone closer to the surface and minimizing the blowing effect.

Moreover, helical pipe flows have the effect of increasing the surface skin friction coefficient. Mishra and Gupta (1979) [20] developed a model for the friction factor correlation for a turbulent flow in helical coils. By combining their model with Marxman and Gilbert (1963) [7], Whitmore et al. (2015) [21] derived an expression used for analytical prediction of the surface skin friction effects in hybrid combustion, and compared it to a series of static firing experiments for different helical port structures listed in Table 1 using gaseous oxygen (GOX)-acrylonitrile butadiene styrene (ABS) motor. Their results presented in Fig. 9 showed an increase of 200-400% of the regression rate depending on the structure, with short pitch helical structure (grain 4) showing the best results. Their analytical prediction however, differed from the experimental results, because it was based only on the skin friction. The observed difference indicated that the blowing effect reduction due to centrifugal flow, is a factor on the increase of the regression rate with a magnitude equivalent or greater than the increase in skin friction.

Previous work on the subject has been conducted by Fuller et al. (2011) [22] using an epoxy-acrylate Watershed® XC 11122 fuel material, and GOX as the oxidizer, investigating complex port geometries including multiport helix grain. Bath (2012) [23] observed the effects of complex port geometries on the fuel burn properties using ABS fuel and nitrous oxide (N_2O) as oxidizer. More recently, Pabarcus (2019) [24] studied the effect of helical port on paraffin fueled hybrid rocket with GOX as the oxidizer.

Note that in contrast to our work, where the helix loop diameter is equal to the pitch of the helix, small helix loop diameter was used in previous studies, meaning that the helical port became cylindrical during the firing test, and didn't maintain its helical structure. Fig. 8 illustrates the fuel port cross section as the port burns and opens up used in [21].

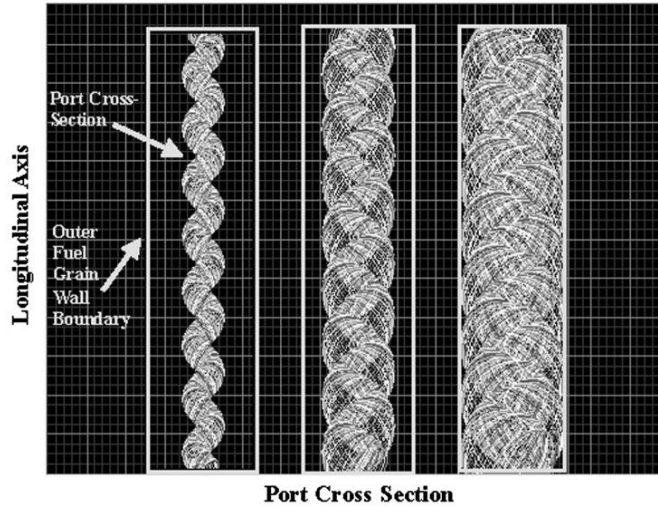


Fig. 8 Fuel port cross section as the port burns and opens up (from left to right). [21]

Table 1 Fuel grain geometry parameters used in [21] static firing experiments. Where the port diameter is d , the helix loop diameter is D_{helix} and the helix pitch is P , as displayed in Fig. 12.

Grain number	Grain length [cm]	Initial port diameter [cm]	Initial helix loop diameter [cm]	Initial helix pitch length [cm]
1	35.98	2.026	-	-
2	35.98	1.524	0.762	15.24
3	35.98	1.524	1.524	15.24
4	22.86	1.524	1.143	2.70

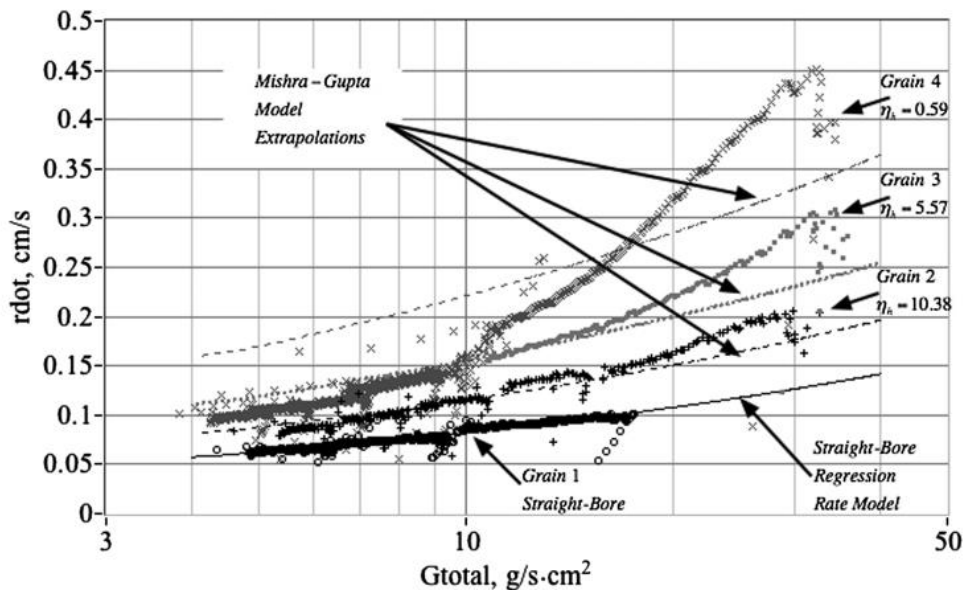


Fig. 9 Regression rate comparison for straight-bore and different helical structures. [21]

The present research focuses on experimental study on the regression rate of a short (35 mm) fuel grain with aggressive 30 mm pitch and 30 mm helix loop diameter. Besides comparing to a straight cylindrical port, the research compares the results of a plain polyester fuel to polyester with addition of 5% expandable graphite, both with a helical port configuration.

2. Experimental set-up and test procedure

Using laboratory scale hybrid rocket system, 12 static fire tests have been conducted to determine the regression rate for helical fuel port. The fuel grains dimensions and port shape were identical in all tests, with half of the fuel grains consisted of plain polyester and the other half of polyester with 5% expandable graphite. Each test employed a different oxidizer (gaseous oxygen) mass flow rate.

2.1 Casting Helical Fuel Port

The fuel grains with helical port were formed by mixing liquid erco® E-7 unsaturated orthophthalic polyester resin together with 1% (of the polyester weight) of hardener (methyl ethyl ketone peroxide). Half of the grains were mixed with 5% (of the total weight) of 100 micron flakes of expandable graphite (Graphit Kropfmühl ES 100 C10). The composition of the polyester used was determined by a chemical analysis to be $C_{42}H_{41}O_{10}$ (molecular structure approximately $CHO_{0.25}$).

The mixture was then poured into an acrylonitrile butadiene styrene (ABS) 3D printed casting mold shown in Fig. 10. After the fuel hardening, the mold was dissolved in acetone as shown in Fig. 11.



Fig. 10 (left) Helical fuel port casting mold; (right) Casted fuel mix, upper row plain polyester, bottom row polyester with 5% EG.



Fig. 11 Dissolving the casting mold

2.2 Experiment Set-Up

The experiment setup included a section of oxidizer injection and ignitor, followed by a cylindrical fuel grain of 35 mm length, having a helical port, with $d = 10 \text{ mm}$ as the initial port diameter, $P = 30 \text{ mm}$ as the helix pitch length, and $D_{helix} = 30 \text{ mm}$ as the helix loop diameter, as shown in Fig. 12. The fuel grain served as both the casing and the combustion chamber. An aft mixing chamber at the end of the fuel grain was attached to a converging nozzle with 6.25 mm throat diameter. During the experiment operation, the thrust, oxygen flow rate into the motor, and the mixing chamber pressure were continuously monitored and recorded. In addition, the motor operation was streamed and recorded by an HD video camera in each test. A general layout of the experimental setup is presented in Fig. 13.

Ignition of the motor was accomplished by a spark plug igniting a short time flammable oxygen-ethylene mix inserted to the ignition section, releasing a substantial amount of heat that enabled the fuel grain to ignite. Every experiment lasted approximately 5 seconds.

In total 12 experiments were conducted using fuel grains with helical port and gaseous oxygen as the oxidizer, six of them made of plain polyester, and the other six formed from polyester and 5% EG mixture. Post burn photos of the fuel grain can be seen in Fig. 14. Each set of experiments (with and without EG) was conducted in different oxidizer mass flow rate to form a graph of the fuel regression rate as function of the oxygen mass flux. The results were compared to previous results made by Eisen and Gany (2021) [25], with addition of three

tests conducted on a short 35mm length grain with a straight port to match high oxidizer mass flux measurements.

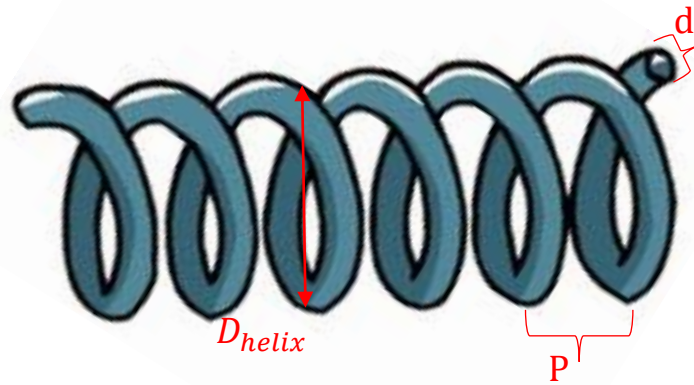


Fig. 12 Schematic description of the helix shape parameters, after [26]

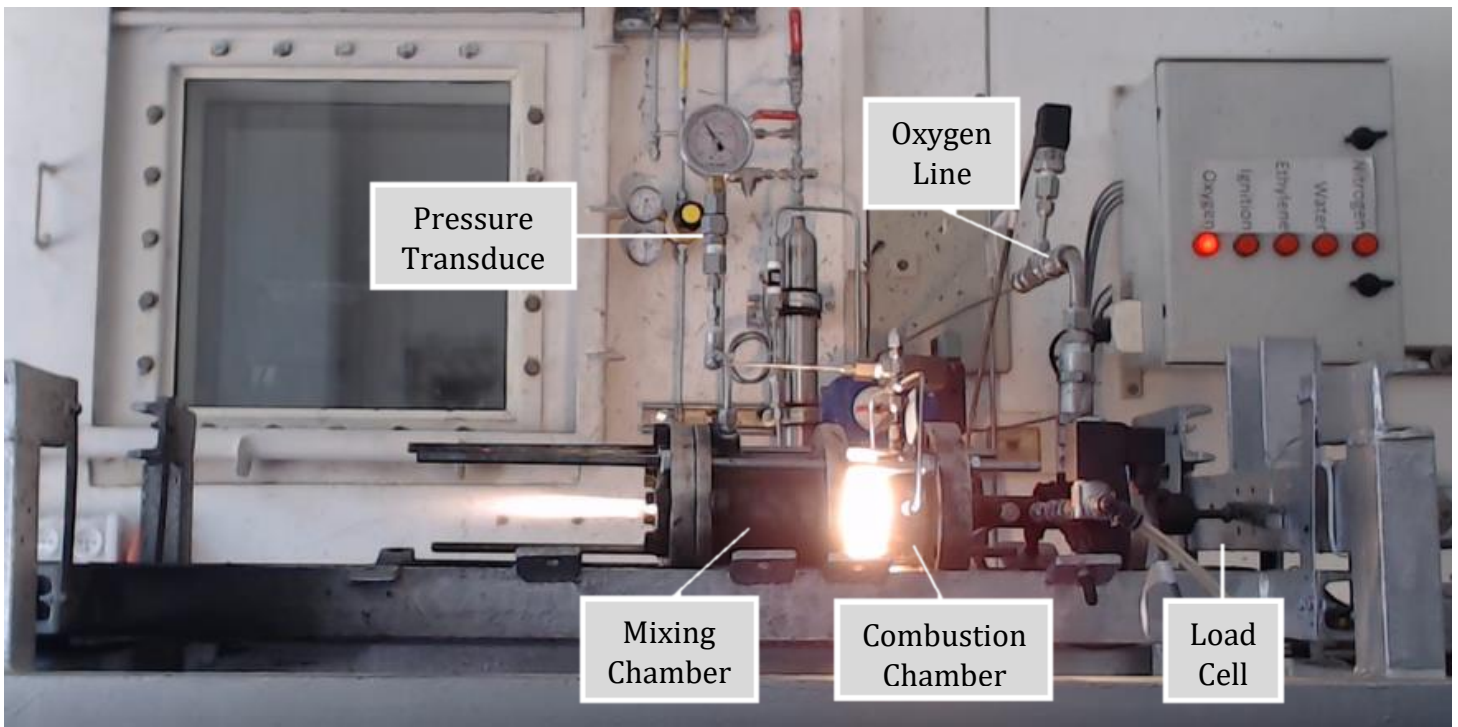


Fig. 13 Photograph of the test set up used for static firing experiments.



Fig. 14 Post burn photos of plain polyester (left) and polyester and 5% EG (right) with helical port.

3. Experimental Results

Measurements of the oxygen mass flow rate during the firing tests were obtained using a choked nozzle at the oxygen line,

$$\dot{m}_{ox} = \frac{P_{ox} A_{ox}}{\sqrt{T}} \sqrt{\frac{\gamma}{R_{ox}}} \left(\frac{2}{\gamma + 1} \right)^{\frac{\gamma+1}{2(\gamma-1)}} \quad (11)$$

where P_{ox} is the oxygen (upstream) pressure, A_{ox} is the choked nozzle throat cross section at the oxygen pipe line, $T = 298 \text{ K}$ assumed to be the ambient room temperature, $R_{ox} = 259.8 \frac{\text{J}}{\text{kg}\cdot\text{K}}$ is the oxygen specific gas constant, and $\gamma = 1.4$ is the specific heat capacity ratio.

The mass of the fuel that was burned was measured by weighing the fuel before and after the firing test,

$$\Delta m = m_i - m_f \quad (12)$$

where m_i and m_f are the fuel grain masses before and after the test, respectively. The average fuel mass flow rate, \dot{m}_{fu} , was calculated by dividing the overall mass loss by the burning time t_b ,

$$\dot{m}_{fu} = \frac{\Delta m}{t_b} \quad (13)$$

The averaged post burn diameter of the port was calculated differently for helical and cylindrical port. For straight cylindrical port,

$$d_f = \sqrt{\left(\frac{4\Delta m}{\pi\rho_{fu}L}\right) + d_i^2} \quad (14)$$

where ρ_{fu} is the fuel density, L is the length of the fuel grain, and d_i and d_f are the initial and final port diameters, respectively.

For the helical port, we divided the calculation into three methods:

3.1 Method 1- Helix Plane

This method provides a way of calculating the effective post-burn port diameter of the helix using volumetric calculation.

From conservation of volume of the fuel grain, the effective post burn port volume ($V_{f,eff}$) can be calculated,

$$V_{f,eff} = \frac{\pi}{4} D^2 L - \frac{m_f}{\rho_{fu}} \quad (15)$$

where D is the fuel grain diameter, L is the length of the fuel grain, m_f is the post burn fuel weight, and ρ_{fu} is the fuel density. Schematic drawing of the volumetric calculation is shown in Fig. 15.

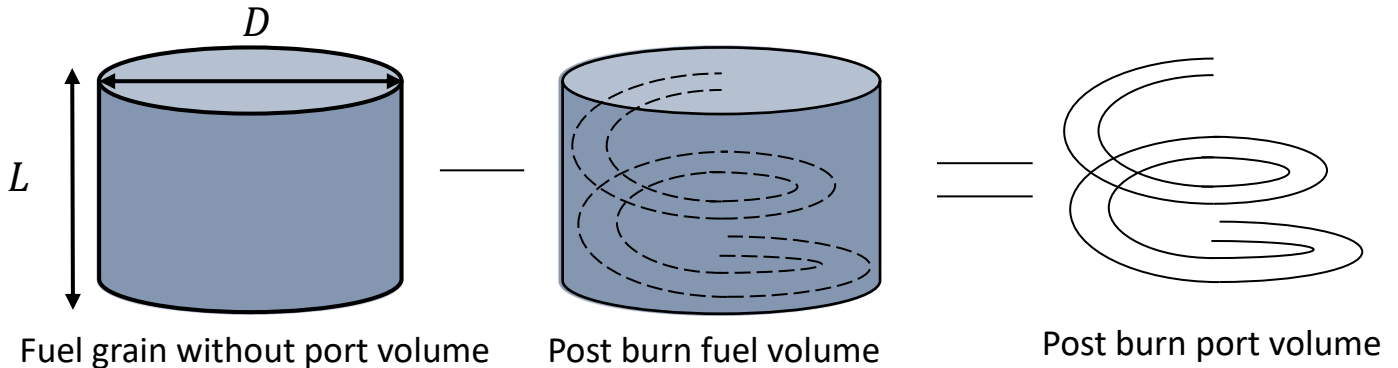


Fig. 15 Schematic drawing of the volumetric calculation

To be able to compare the regression rate to that of a straight cylindrical port the effective cross section area of the fuel port needs to be projected to the fuel plane. Introducing the lead angle λ , the angle between the tangent to a helix and

the plane perpendicular to the helical axis (fuel plain), schematic description of lead angle is shown in Fig. 16.

$$\lambda = \arctan\left(\frac{P}{D_{helix}}\right) \quad (16)$$

For the helix shape used in this paper the lead angle is,

$$\lambda = \arctan\left(\frac{30}{30 \cdot \pi}\right) = \arctan\left(\frac{1}{\pi}\right) \quad (17)$$

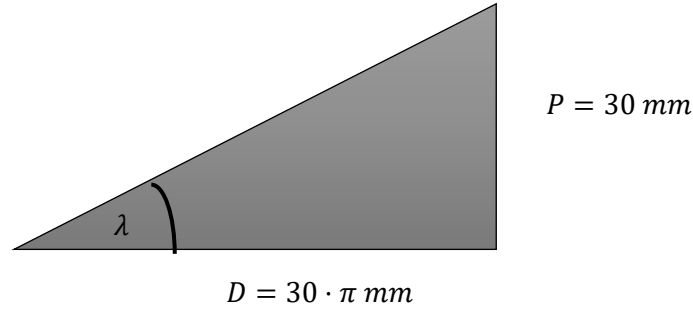


Fig. 16 Schematic description of lead angle.

Using the lead angle, the effective post burn cross section area projected to the fuel plain $A_{f,eff}$ can be calculated,

$$A_{f,eff} = \left(\frac{\pi}{4}D^2 - \frac{m_f}{\rho_{fu}L}\right) \sin(\lambda) \quad (18)$$

The effective post-burn diameter $d_{f,eff}$,

$$d_{f,eff} = \sqrt{\frac{4}{\pi} \cdot A_{f,eff}} \quad (19)$$

3.2 Method 2- Straight Port Analogy

This method will show the effect of the enhancement of the regression rate due to the helical shape and not due the addition in port length. The helical port structure used in the experiments has pitch that is equal to the loop diameter. Thus, the port length for a helical port, l_{port} can be calculated using Pythagoras theorem,

$$l_{port} = L \cdot \sqrt{\pi^2 + 1} \quad (20)$$

By accounting for the increase in length due to helical port, the regression rate can be calculated the same way as a straight cylindrical port using **שגיאה! מקור** **ההפניה לא נמצא.**

$$d_f = \sqrt{\left(\frac{4\Delta m}{\pi\rho_{fu}l_{port}}\right) + d_i^2} \quad (21)$$

The average regression rate \dot{r} and the oxidizer mass flux were calculated as follows,

$$\dot{r} = \frac{d_f - d_i}{2t_b} \quad (22)$$

$$G_{ox} = \frac{16\dot{m}_{ox}}{\pi(d_i + d_f)^2} \quad (23)$$

For method 1 we used $d_{f,eff}$ instead of d_f in the calculation of the average regression rate only, while using method 2 to calculate the oxidizer mass flux. For straight cylindrical port and method 2 we used d_f from Eq. (14) and Eq. (23) respectively for the calculation of \dot{r} and G_{ox} . \dot{m}_{ox} was constantly recorded during the firing tests and calculated according to Eq. (11).

3.3 Method 3- Grain Parameters

This method of calculation will focus on the overall grain size, meaning the length used for calculation is the fuel grain length, L . Furthermore, to account for the helix shape, we used a corrected initial port diameter $d_{i,cor}$, accounting for the initial mass loss due to the longer port structure.

$$d_{i,cor} = d_i \cdot (\pi^2 + 1)^{\frac{1}{4}} \quad (24)$$

Using Eq. (15), the post burn diameter,

$$d_f = \sqrt{D^2 - \frac{4m_f}{\pi\rho_{fu}L}} \quad (25)$$

The average regression rate \dot{r} and the oxidizer mass flux G_{ox} were calculated as follows,

$$\dot{r} = \frac{d_f - d_{i,cor}}{2t_b} \quad (26)$$

$$G_{ox} = \frac{16\dot{m}_{ox}}{\pi(d_i + d_f)^2} \quad (27)$$

where the G_{ox} , d_i and d_f are the same as calculated in method 2.

Experimental results of the regression rate for three types of fuels and configurations (plain polyester with helical port, polyester + 5% EG with helical port, and plain polyester with straight cylinder port) for methods 1, 2 and 3 is presented in Fig. 17, Fig. 18, and Fig. 19, respectively.

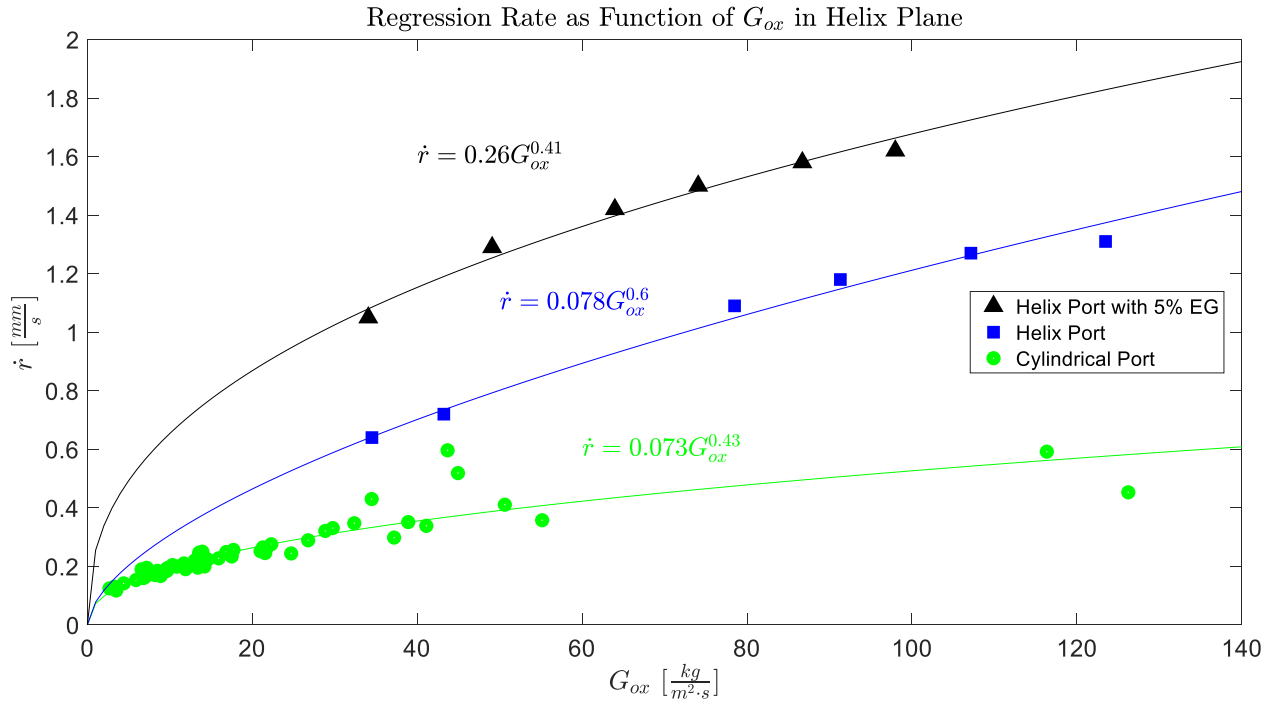


Fig. 17 regression rate \dot{r} vs oxidizer (oxygen) mass flux G_{ox} for polyester with a helical port, polyester and 5% EG with a helical port, and polyester with a straight cylindrical port, using helix plane method.

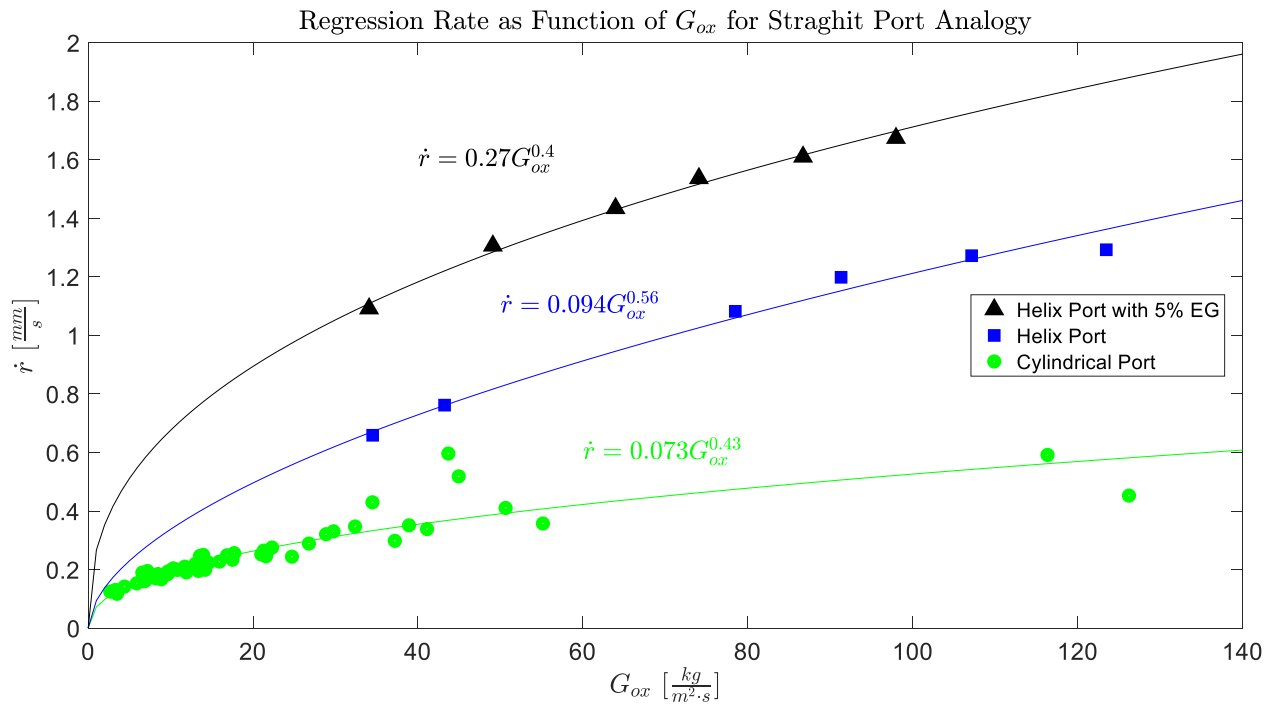


Fig. 18 regression rate \dot{r} vs oxidizer (oxygen) mass flux G_{ox} for polyester with a helical port, polyester and 5% EG with a helical port, and polyester with a straight cylindrical port, using straight port analogy method.

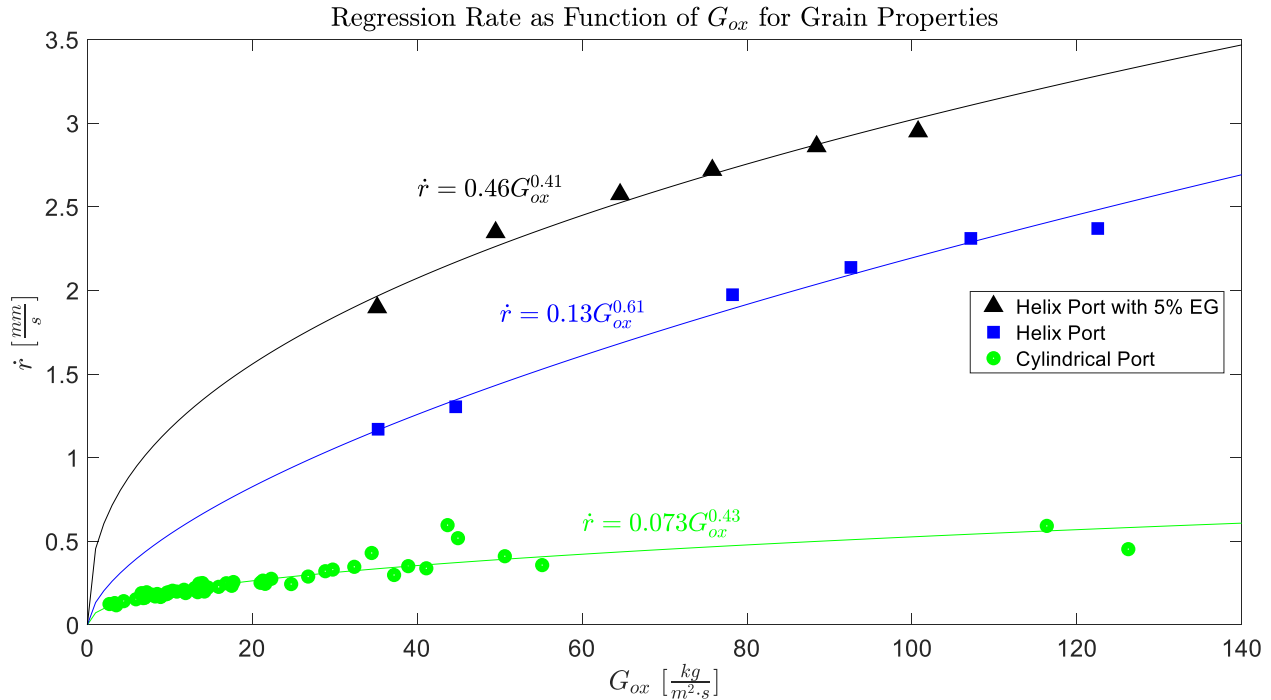


Fig. 19 regression rate \dot{r} vs oxidizer (oxygen) mass flux G_{ox} for polyester with a helical port, polyester and 5% EG with a helical port, and polyester with a straight cylindrical port, using grain parameters method.

The experimental results clearly show the increase in regression rate due to the helical port shape and the addition of EG. In all cases, the fuel regression rate showed an increase with increasing the oxygen mass flux. For methods 1 and 2 very small changes between the regression rate correlation is observed. At the lower oxygen mass fluxes, the helical port structure increased the regression rate by 2-fold, and with the addition of 5% EG, an increase of 3-fold is shown. For high mass flux range, for plain polyester an increase of up to 2.5-folds is shown, and for polyester + 5% EG the regression rate was increased by 3-fold. Similar behavior to plain polyester is also reported by Whitmore et al. (2015) [21] for ABS fuel with the use of helical port with small helix loop diameter.

By taking into account only the overall fuel grain size in method 3, even larger apparent increase in the regression rate was noticed, up to 4-folds for plain polyester and 6-fold for 5% EG. The meaning for the designer is, that when considering the size of the fuel and not the inner structure of the grain, we get even larger increase in the regression rate due to a helical port. Table 2 summarizes the regression rate empirical correlations obtained from the experiments.

Table 2: comparison of fuel regression rate empirical correlations for plain polyester and polyester + 5% EG with helical port, as well as plain polyester with a straight cylindrical port, with gaseous oxygen as the oxidizer for different methods of calculation (\dot{r} in mm/s , G_{ox} in $kg/s \cdot m^2$).

Fuel	Regression rate empirical correlation		
	Method 1- Helix Plane	Method 2- Straight Port Analogy	Method 3-grain parameters
Plain polyester with cylindrical port	$\dot{r} = 0.073G_{ox}^{0.43}$	$\dot{r} = 0.073G_{ox}^{0.43}$	$\dot{r} = 0.073G_{ox}^{0.43}$
Plain polyester with helical port	$\dot{r} = 0.078G_{ox}^{0.6}$	$\dot{r} = 0.094G_{ox}^{0.56}$	$\dot{r} = 0.13G_{ox}^{0.61}$
Polyester + 5% EG with helical port	$\dot{r} = 0.26G_{ox}^{0.41}$	$\dot{r} = 0.27G_{ox}^{0.4}$	$\dot{r} = 0.46G_{ox}^{0.41}$

4. Conclusions

A fairly new concept of increasing the fuel regression rate in a hybrid motor with a helical port structure was investigated experimentally in a series of static firing tests using gaseous oxygen as the oxidizer. The implementation of this concept for plain polyester showed an increase of up to 2.5 fold in the regression rate compared to a straight cylindrical port, whereas with the addition of 5% expandable graphite an increase of 3-fold in the regression rate was measured. By relating the regression rate to the fuel grain size (length), even larger increase in the regression rate was noticed, up to 4-folds for plain polyester and 6-fold for 5% EG. In addition, with the use of a helical port structure the ratio between the fuel mass flow rate and the fuel overall grain size increases due to lengthening of the internal flow path for a given fuel grain length. Its practical meaning is that one can obtain a substantially greater thrust from a given fuel grain geometry or alternatively noticeably shortening the fuel grain for the same thrust.

References

- [1] Hybrid rocket engine <https://www.sciencelearn.org.nz/images/412-hybrid-rocket-engine>
- [2] Altman, D., and Holzman, A., "Overview and History of Hybrid Rocket Propulsion," Fundamentals of Hybrid Rocket Combustion and Propulsion, edited by M.J. Chiaverini and K. K. Kuo, Vol. 218, Progress in Astronautics and Aeronautics, AIAA, Reston, VA, Vol. 218, 2007, pp. 1-36.
- [3] Sharp, T. 2019. SpaceShipOne: The first private spacecraft. <http://www.space.com/16769-spaceshipone-first-private-spacecraft.html>
- [4] Howell, E. 2019. SpaceShipTwo: A flight path to space tourism. <https://www.space.com/19021-spaceshiptwo.html>
- [5] Calabro, M. "Overview on hybrid propulsion." Progress in Propulsion Physics, 2011, pp. 353-374. <https://doi.org/10.1051/eucass/201102353>.
- [6] Cantwell, B., Karabeyoglu, A., and Altman, D., "Recent advances in hybrid propulsion," International Journal of Energetic Materials and Chemical Propulsion, Vol. 9, No. 4 2010, pp. 305-326. <https://doi.org/10.1615/intjenergeticmaterialschemprop.v9.i4.20>
- [7] Marxman, G., and Gilbert, M., "Turbulent Boundary Layer Combustion in the Hybrid Rocket," International Symposium of Combustion, Vol. 9, No. 1, 1963, pp. 371-383. [https://doi.org/10.1016/s0082-0784\(63\)80046-6](https://doi.org/10.1016/s0082-0784(63)80046-6)
- [8] Evans, B., Risha, G., Favorito, N., Boyer, E., Wehrman, R., Libis, N., and Kuo, K., "Instantaneous regression rate determination of a cylindrical x-ray transparent hybrid rocket motor," 39th AIAA/ASME/SAE/ASEE Joint Propulsion Conference and Exhibit, pp. 1-11, 2003. <https://doi.org/10.2514/6.2003-4592>.
- [9] Evans, B., Favorito, N., and Kuo, K., "Study of solid fuel burning-rate enhancement behavior in an X-ray translucent hybrid rocket motor," 41st AIAA/ASME/SAE/ASEE Joint Propulsion Conference & Exhibit, pp. 1-13, 2005. <https://doi.org/10.2514/6.2005-3909>.
- [10] Karabeyoglu, M., Cantwell, B., and Altman, D., "Development and testing of paraffin-based hybrid rocket fuels," 37th Joint Propulsion Conference and

Exhibit, 2001.

<https://doi.org/10.2514/6.2001-4503>.

- [11] Karabeyoglu, M. A., Altman, D., and Cantwell, B. J., "Combustion of liquefying hybrid propellants: Part 1, general theory," *Journal of Propulsion and Power*, Vol. 18, No. 3, 2002, pp. 610–620.
<https://doi.org/10.2514/2.5975>.
- [12] Karabeyoglu, A., Ziliac, G., Cantwell, B. J., DeZilwa, S., and Castellucci, P., "Scale-up tests of high regression rate paraffin-based hybrid rocket fuels," *Journal of Propulsion and Power*, Vol. 20, No. 6, 2004, pp. 1037–1045.
<https://doi.org/10.2514/1.3340>
- [13] Karabeyoglu, M. A., and Cantwell, B. J., "Combustion of liquefying hybrid propellants: Part 2, stability of liquid films," *Journal of Propulsion and Power*, Vol. 18, No. 3, 2002, pp. 621–630.
<https://doi.org/10.2514/2.5976>.
- [14] Weinstein, A., and Gany, A., "Investigation of paraffin-based fuels in hybrid combustors," *International Journal of Energetic Materials and Chemical Propulsion*, Vol. 10, No. 4, 2011, pp. 277–296.
<https://doi.org/10.1615/intjenergeticmaterialschemprop.2012001394>.
- [15] Sisi, S., and Gany, A., "Combustion of plain and reinforced paraffin with nitrous oxide," *International Journal of Energetic Materials and Chemical Propulsion*, Vol. 14, No. 4, 2015, pp. 331–345.
<https://doi.org/10.1615/intjenergeticmaterialschemprop.2015011139>.
- [16] Ben-Basat (Sisi), S., and Gany, A., "Heat and mass transfer analysis for paraffin/nitrous oxide burning rate in hybrid propulsion," *Acta Astronautica*, Vol. 120, 2016, pp. 121–128.
<https://doi.org/10.1016/j.actaastro.2015.12.011>.
- [17] Elanjickal, S., and Gany, A., "Enhancement of the fuel regression rate in hybrid propulsion by expandable graphite additive," *Combustion Science and Technology*, Vol. 192, No. 7, 2020, pp. 1253–1273.
<https://doi.org/10.1080/00102202.2020.1748017>.
- [18] Muller, G. T., and Gany, A., "Burning phenomena of a polymeric fuel containing expandable graphite," *Propellants, Explosives, Pyrotechnics*, Vol. 45, No 11, 2020, pp. 1764–1768.
<https://doi.org/10.1002/prop.202000138>.
- [19] Muller, G. T., and Gany, A., "Expandable graphite effect on solid fuel and propellant combustion," *FirePhysChem*, Vol. 2, No.1 2022, pp. 72–75.
<https://doi.org/10.1016/j.fpc.2021.12.001>.

- [20] Mishra, P., and Gupta, S. N., "Momentum transfer in curved pipes. 1. newtonian fluids," *Industrial & Engineering Chemistry Process Design and Development*, Vol. 18, No 1. 1979, pp. 130–137.
<https://doi.org/10.1021/i260069a017>
- [21] Whitmore, S. A., Walker, S. D., Merkley, D. P., and Sobbi, M., "High regression rate hybrid rocket fuel grains with helical port structures," *Journal of Propulsion and Power*, Vol. 31, No 6, 2015, pp. 1727–1738.
<https://doi.org/10.2514/1.b35615>.
- [22] Fuller, J., Ehrlich, D., Lu, P., Jansen, R., and Hoffman, J., "Advantages of rapid prototyping for hybrid rocket motor fuel grain fabrication," 47th AIAA/ASME/SAE/ASEE Joint Propulsion Conference & Exhibit, 2011.
<https://doi.org/10.2514/6.2011-5821>.
- [23] Bath, A., "Performance Characterization of Complex Fuel Port Geometries for Hybrid Rocket Fuel Grains," M.S. Thesis, College of Engineering and Applied Sciences, Utah State University, Logan, UT, 2012.
- [24] Pabarcus, L., "Development and preliminary testing of paraffin hybrid rocket fuel grains with helical port structures," AIAA Propulsion and Energy 2019 Forum, 2019.
<https://doi.org/10.2514/6.2019-4187>.
- [25] Eisen, N. E., and Gany, A., "Investigation of a marine water-breathing hybrid ram-rocket motor," *Journal of Propulsion and Power*, Vol. 38, No. 3, 2021, pp. 370–377.
<https://doi.org/10.2514/1.b38590>.
- [26] Helix <https://scribblenauts.fandom.com/wiki/Helix>